GEOPHYSICAL RESEARCH LETTERS, VOL. ???, XXXX, DOI:10.1029/,

High-altitude gravity waves in the Martian thermosphere observed by MAVEN/NGIMS and modeled by a gravity wave scheme

Erdal Yiğit[1], Scott L. England[2], Guiping Liu[2], Alexander S. Medvedev[3,4],

Paul R. Mahaffy[5], Takeshi Kuroda[6], Bruce M. Jakosky[7]

Corresponding author: E. Yiğit, George Mason University, Department of Physics and Astronomy, Space Weather Group, MSN:3F3, Fairfax, VA 22030, USA. (eyigit@gmu.edu)

[1]George Mason University, Department of Physics and Astronomy, Fairfax, VA, USA.

[2]University of California, Berkeley, Space Sciences Laboratory, Berkeley, CA, USA.

[3]Max Planck Institute for Solar System Research, Göttingen, Germany.

[4]Institute of Astrophysics, Georg-August University, Göttingen, Germany.

[5]NASA, Goddard Space Flight Center, Greenbelt, MA, USA.

[6]Department of Geophysics, Tohoku University, Sendai, Japan.

[7]Laboratory for Atmospheric and Space Physics, University of Colorado, USA.

First high-altitude observations of gravity wave (GW)-induced CO_2 density perturbations in the Martian thermosphere retrieved from NASA's NGIMS instrument on board the MAVEN satellite are presented and interpreted using the extended GW parameterization of *Yiğit et al.* [2008] and the Mars Climate Database as an input. Observed relative density perturbations between 180–220 km of 20–40% demonstrate appreciable local time, latitude, and altitude variations. Modeling for the spatiotemporal conditions of the MAVEN observations suggests that GWs can directly propagate from the lower atmosphere to the thermosphere, produce appreciable dynamical effects, and likely contribute to the observed fluctuations. Modeled effects are somewhat smaller than the observed but their highly variable nature is in qualitative agreement with observations. Possible reasons for discrepancies between modeling and measurements are discussed.

1. Introduction

Internal gravity waves (GWs) are fundamental features of all stably stratified planetary atmospheres. On Earth, they are primarily generated by lower atmospheric meteorological processes, and have profound dynamical and thermal effects on the circulation of the middle and upper atmosphere [e.g., *Yiğit et al.*, 2009]. A contemporary review of the role of internal wave processes in Earth's atmosphere can be found in the work by *Yiğit and Medvedev* [2015] and in the book by *Yiğit* [2015, Chapter 5]. On Mars, GWs of lower atmospheric origin play a similar important dynamical [*Medvedev et al.*, 2011a] and thermal role [*Medvedev and Yiğit*, 2012] in the upper atmosphere. While global modeling demonstrates a direct influence of GWs on the large-scale Martian circulation, observations have provided a valuable insight into various GW structures. Although the effect of waves cannot be directly measured, GW signatures, for example, small-scale density perturbations have been detected during aerobraking on Mars Global Surveyor and Mars Odyssey [e.g., *Fritts et al.*, 2006]. Such measurements have shown that magnitudes of GW-induced perturbations vary between 5–50%.

NASA's Mars Atmosphere Volatile EvolutioN (MAVEN) mission was launched in November 2013 and entered Mars' orbit in September 2014. Its prime goal is to explore the Martian upper atmosphere in an unprecedented manner and to help better understand Mars atmospheric loss processes and coupling to the solar wind. In this study, we analyze the first CO_2 density data from the Neutral Gas Ion Mass Spectrometer (NGIMS) instrument on board the MAVEN satellite for high-altitude gravity wave signatures, and interpret these results by calculating for the spatiotemporal conditions of the observa-

tions the fluctuations associated with the propagation of lower atmospheric GWs into the thermosphere and the direct effects resulting from their dissipation. For this, the GW parameterization of *Yiğit et al.* [2008] is used together with the Mars Climate Database (MCD) atmospheric fields.

Next section presents the MAVEN data and the analysis method; section 3 outlines the GW scheme that calculates the direct GW propagation in the Martian whole atmosphere; sections 4 and 5 present the observed density fluctuations and the modeled GW effects and fluctuations, respectively. Summary and conclusions are given in section 6.

2. MAVEN/NGIMS Data & Analysis Method

The NGIMS instrument on board the MAVEN satellite is a quadrupole mass spectrometer designed to measure the density of the gas in Mars' upper atmosphere between 2 and 150 Daltons with unit mass resolution [*Mahaffy et al.*, 2014]. It has an open and a closed source channel, both of which are used to measure the neutral density when MAVEN is below 500 km altitude, relative to the areoid. Both channels can be used to measure the density of CO_2, which is a useful proxy for the total mass density at altitudes below $\sim$250 km.

This study uses the Level 2 (version 3, revision 1) of the NGIMS data, in which the instrument counts in each mass channel have been combined, knowing the fractionation patterns of CO_2, into a mass density for this species. Further, the effect of the transition from the unattenuated instrument counts at high altitudes to the attenuated instrument counts at lower altitudes has been accounted for, using data from an altitude when both the attenuated and unattenuated signals are within the appropriate range. The analysis

presented here will focus on determining atmospheric density perturbations seen in either one of open or close source channels. As such, any uncertainties in the differences between these channels, how densities are computed from either channel, any uncertainty in the fractionation of CO_2, or any inbound/outbound asymmetry resulting from the pile-up effect do not affect the analysis presented here. Given that the NGIMS instrument sweeps across all mass channels with a 4 s cadence, it can be used to identify perturbations with spatial scales larger than ∼20 km along the spacecraft track. With an orbital speed of ∼ 4.2 km s^{-1} the geometry of this sampling varies during the 12 minutes that the spacecraft spends at altitudes below 250 km. Close to periapsis, the spacecraft is moving almost entirely parallel to the areoid, and thus would be sampling only horizontal structures (wavelengths) as it moves, whereas at higher spacecraft altitudes there is an increasing vertical component to its motion, and as such vertical structures (wavelengths) will become increasingly important in any signal seen by this instrument.

Figure 1a shows the CO_2 density measurements from a typical periapsis pass. For this particular orbit, periapsis was at 153 km above the areoid, at 74°N, 179°E, 4.2 hours local time and 259° solar longitude. The total time that the spacecraft is below 250 km above the areoid is 710 s. Examining the overall structure of the CO_2 density profile during this periapsis pass, a clear increase in CO_2 density with decreasing spacecraft altitude can be seen. However, superimposed on this trend are significant, quasi-oscillatory perturbations in the density, whose amplitudes also increase towards periapsis. These perturbations are visible at spacecraft altitudes from periapsis (153 km) up to around 200 km, which is several scale heights above the altitude where GWs have been seen

in previous thermospheric observations at Mars. For example, *Tolson et al.* [2007] had reported wave observations between ∼100–140 km altitude.

To identify the perturbations, an estimate of the background density profile is necessary. Previous analysis of similar in situ observations have done this using a variety of techniques including a long running mean [e. g., *Kasprzak et al.*, 1988], and a least-squares polynomial fit [e. g., *Snowden et al.*, 2013]. The green line on Figure 1a shows a 7th order polynomial fit to the log of the density observations, which provides a good estimate of the background mean density and allows for (1) fitting the overall density increase towards periapsis, (2) changes in the scale height (and therefore temperature) of the background over the altitude range fitted, and (3) for asymmetry between the inbound and outbound density measurements resulting from differences in the sampling latitude, longitude and local time between the inbound and outbound portions of the periapsis pass and any signature instrumental sampling artifacts. Removing this background from the observations provides an estimate of the density perturbation, which is then normalized against the background density to provide an estimate of the fractional density perturbation ($\Delta\rho/\bar{\rho} = \rho'/\rho_0$). This is shown for the same periapsis pass in Figure 1b. The associated density perturbations are quasi-oscillatory, having a range of amplitudes of order $10 - 100\%$ of the background mean density and exist throughout the entire periapsis pass, although both the count rate of the instrument and the ability to fit to the background density decrease with increasing altitude. For this reason, we will limit the analysis of these perturbations to observations taken below 220 km altitude (∼50–650 s during this periapsis pass), and focus primarily on observations taken below 200

km altitude (∼100–600 s during this periapsis pass). Further, as these perturbations are quasi-oscillatory, with spatial scales of tens to hundreds km along the satellite track, the assumption that they are associated with atmospheric GWs will be made in all subsequent analysis, following previous studies [e.g., *Kasprzak et al.*, 1988; *Fritts et al.*, 2006; *Tolson et al.*, 2007]. While there is likely some component of the observed density perturbation not associated with such waves, if GWs dominate these observations, the mean behavior of the density perturbations is expected to follow that of the atmospheric GWs in this region. For this reason, all subsequent analysis will determine the mean properties of these density perturbations over a region of the Martian thermosphere.

This study focuses on data taken during December 2014. During this time period, there was a latitudinally-symmetric coverage in the middle-to-high Northern latitudes as the MAVEN spacecraft moved from day to night across the dawn terminator during the periapsis passes. This allowed us to look for day-to-night variations in GWs, which happened to be one of the key objectives from the Venus Express Orbiter Neutral Mass Spectrometer (ONMS) data [e.g., *Kasprzak et al.*, 1988]. Finally, the periapsis altitude remained approximately constant during this time period, which enables the averaging of the data from this entire time interval to compute the mean amplitude of the observed GWs and their variation. In total, there are 78 periapsis data sets for which good quality Level 2 densities are available during the time period covering 1–23 December for the closed source data, and 1–18 December for the open source data. The altitude, local time and latitude coverage of these data is shown in Figures 1c and 1d. To calculate the mean properties of the observed GWs, the region over which data were averaged was chosen

based on the coverage shown in Figures 1c and 1d to avoid any sampling bias, such as the correlation between altitude and latitude which would occur if the entire data set were used.

3. The Extended Gravity Wave Scheme

The extended spectral nonlinear gravity wave parameterization of *Yiğit et al.* [2008] is employed here for quantifying the direct propagation of lower atmospheric GWs into the Martian thermosphere. Mars Climate Database fields (meridional and zonal wind velocities, density, and temperature) appropriate for the spatiotemporal conditions of the presented MAVEN observations are used as an input in order to drive the extended parameterization and calculate the GW-induced zonal gravity wave drag as well as wind and density fluctuations.

The extended GW parameterization, developed originally for Earth's whole atmosphere system models, is described in detail in the work by *Yiğit et al.* [2008]. Its implementation and application to modeling Mars' atmosphere is given in the papers by *Medvedev et al.* [2011b, a]. The scheme is appropriate for planetary whole atmosphere numerical models extending from the lower atmosphere into the thermosphere. Its extensive use in general circulation modeling of the terrestrial [*Yiğit et al.*, 2009, 2012, 2014; *Yiğit and Medvedev*, 2009, 2010] and Martian [*Medvedev and Yiğit*, 2012; *Medvedev et al.*, 2013, 2015; *Yiğit et al.*, 2015] atmosphere demonstrated an appreciable vertical coupling by gravity waves in both planets, and have thus helped to quantify wave-mean flow interactions there. Application of this scheme has allowed a Martian general circulation model to reproduce for the

first time the latitudinal temperature profile derived from the aerobraking measurements of *Bougher et al.* [2006].

The gravity wave scheme calculates vertical propagation and evolution of small-scale wave harmonics systematically accounting for the major wave dissipation mechanisms in the Martian atmosphere: due to nonlinear breaking/saturation, molecular viscosity and thermal conduction. An empirical distribution of GW spectrum is specified at the source level in the lower atmosphere with a GW horizontal wavelength of $\lambda_H = 250$ km and a source strength of $\overline{u'w'}_{max} = 0.0025$ m^2 s^{-2}, as described by *Medvedev et al.* [2011b], and the scheme calculates at consecutive vertical levels the momentum and temperature tendencies imposed by GWs on the larger-scale atmospheric flow. In this study, we use the same GW source specification (constrained with the radio occultation data of *Creasey et al.* [2006a]) as in the previous works [*Medvedev and Yiğit*, 2012; *Medvedev et al.*, 2013]. Therefore, our modeling framework can provide a first-order estimate of how much lower atmospheric GWs contribute to the observed high-altitude density fluctuations. We next present the observations of GW signatures by MAVEN, and then discuss the relevant modeling results.

4. MAVEN Observations of CO_2 Density Fluctuations

Despite the relatively constant observing geometry, substantial variations in the gravity wave density perturbations along the spacecraft track are seen over the 78 periapsis datasets taken during December 2014 as described in Section 2 and shown in Figure 1a. GW signatures can be highly localized and variable [e.g., *Creasey et al.*, 2006b; *Fritts et al.*, 2006]; additionally the in situ sampling of the NGIMS instrument is of local nature.

Thus, rather than focusing on the samples seen in individual orbits, which are subject to significant geometric effects, the following analysis will focus on the mean properties observed within a volume. With the number of samples available during December 2014, this allows the variations in gravity wave amplitudes with latitude, local time and altitude to be determined over a region that has never been studied before at Mars.

To determine the local-time variation in gravity wave amplitudes, all data from 180-200 km altitude, and from 62°-75° latitude are selected (shown by the red box in Figure 1d). The upper limit of 200 km is selected to stay within the altitude range of both high CO_2 counting rate (clear signal of the perturbations), and within the region where the background density profile can be fit well. The lower limit of 180 km is chosen to restrict the data to a region of approximately constant spacecraft velocity vector relative to the surface (i.e., away form periapsis where the spacecraft is sampling horizontal variations only). The latitude range is selected to allow for even sampling in latitude and altitude (see Figure 1d). Figure 2b shows with the solid line the mean values of the absolute relative density perturbation (ρ'/ρ_0) within this volume, in 1-hour local time (LT) bins. A clear increase in the wave amplitudes is seen with decreasing LT from a value of ∼20% at 9-10 hours LT, to 40% at 2–3 hours LT. This factor of two increase from day to night is comparable to that found with the ONMS mass spectrometer observations on Pioneer Venus [*Kasprzak et al.*, 1988]. The continuity equation implies that the density perturbations resulting from GWs are the result of a combination of vertical advection and adiabatic expansion. *Genio et al.* [1978] have argued that for heavy species such as CO_2, whose density decreases rapidly with altitude, the effect of vertical advection

dominates. This effect is inversely proportional to the density scale height H. Figure 2b shows the variation of the CO_2 scale height with local time (dashed line). The mean CO_2 scale height on the dayside is approximately twice that of the nightside. Thus, one would expect the relative density amplitudes on the dayside to be around half that of the nightside, which is consistent with the NGIMS observations.

To determine the latitudinal variation in GW amplitudes, all data from 190–200 km altitude, and from 60°–75°N latitude are selected (shown by the green box in Figure 1d). This range is chosen to maximize the latitude range, while eliminating any correlation between altitude and latitude within the chosen volume. Figure 2c shows the mean values of the absolute relative density perturbation over this range in 2.5° latitude bins. A simple trend in the wave amplitudes with latitude is not seen, but the amplitudes are somewhat lower in the 60°-65° latitude region (∼20% relative density perturbation) compared with the region above 65°N latitude (∼30-40% relative density perturbation). Given that a comparatively small range of latitude is sampled, it is possible that a more systematic latitudinal variation could be present. However, owing to the precession of the MAVEN spacecraft orbit, it is not possible to decouple the latitudinal and local time variations in the observations over any other subsequent portion of its orbit so-far, limiting this analysis to just December 2014 and thus this relatively small latitude range.

To determine the altitude variation in GW amplitudes, all data from 180–220 km altitude, and from 62°-70° latitude are selected (shown by the blue box in Figure 1d). This range is chosen to maximize the altitude range, while eliminating any correlation between the altitude and latitude within the chosen volume. Figure 2c shows the altitude variation

of the mean ρ'/ρ_0 in 5 km altitude bins: ρ'/ρ_0 increases from ∼25% to 35% up to 200 km level, around which ρ'/ρ_0 is approximately constant. Above 200 km ρ'/ρ_0 decreases down to 20%. These results suggest that for the observed waves for $z < 200$ km exponential amplitude growth dominates over dissipation, while for $z > 200$ km wave dissipating becomes more dominant, leading to weaker relative fluctuations.

Overall, these results indicate that the thermosphere is characterized by strong dissipation of gravity waves and deposition of their energy into the background atmosphere. This result is consistent with observations from lower altitudes in the thermosphere, such as *Fritts et al.* [2006], who presented evidence for strong gravity wave dissipation in the 100–140 km altitude region. Modeling studies have demonstrated strong GW dissipation in the Martian lower thermosphere [e.g., *Medvedev et al.*, 2011a; *Medvedev and Yiğit*, 2012]. Our results suggest that such dissipative processes and the associated wave dynamical and thermal impact on the global circulation can extend to much higher altitudes.

A longitudinal variation in the gravity wave amplitudes, similar to that reported by *Fritts et al.* [2006], was investigated using the December 2014 NGIMS dataset (not shown), but no clear trend was found. It is possible that this is a result of the higher altitude of the NGIMS observations, the limited number of samples, or the time-period and latitude selected.

5. Modeling Gravity Wave-Induced Effects on Mars

To provide a further perspective to the interpretations of observed density fluctuations, we next model the direct propagation of lower atmospheric GWs into the Martian thermosphere with the extended nonlinear GW scheme of *Yiğit et al.* [2008]. Using the MCD

atmospheric fields chosen for the MAVEN spatiotemporal conditions as an input to the GW scheme, we assess the contribution of lower atmospheric GWs to the observed density fluctuations.

Figure 3 shows all the calculated instantaneous altitude profiles of (a) the zonal GW drag a_x, (b) the root-mean square (rms) horizontal wind fluctuations u', and (c) the relative density perturbations ρ'/ρ_0 modeled for MAVEN observational conditions. While the modeled GW drag can be interpreted as representative of the wave dynamical effects on the atmospheric circulation, u' provides an insight into the propagation depth of small-scale GWs into the thermosphere. Overall, GWs propagate to high altitudes (up to $\sim$200 km) and produce substantial drag of up to $\sim$–10^5 m s^{-1} day^{-1}, peaking between 100 and 160 km. The associated wind fluctuations, typically peaking around the same heights as well, can reach up to 350 m s^{-1}. The resulting relative density fluctuations can reach instantaneously up to 180% around 100 km. Overall, in regions of strong GW activity (large u'), wave-induced acceleration/deceleration, which depends also on the rate of vertical wave damping, and density fluctuations are, generally, larger. *Fritts et al.* [2006]'s analysis of MGS and ODY aerobraking density data showed significant (from tens to over 100 percent) GW-induced density fluctuations between 100 and 140 km. As seen, our simulation results are in a very good agreement with the observations of *Fritts et al.* [2006] in this altitude range.

The average values of GW effects are also shown in Figure 3 with the yellow dashed lines for each parameter. The peak mean values are situated around 100 km with $a_x = -2000$

m s^{-1} day^{-1}, $u' = 100$ m s^{-1}, and $\rho'/\rho_0 \approx 70\%$. It is seen that large departures can occur from the mean quantities.

These results demonstrate that GWs propagate very high, and their effects (as a consequence of wave dissipation) are spatiotemporally very large. In the lower atmosphere below $\sim$ 50 km, GW dissipation is generally small, and individual harmonics achieve large amplitudes as they arrive at higher altitudes, where they are gradually obliterated by the increasing nonlinear damping, molecular diffusion and thermal conduction [*Yiğit et al.*, 2008; *Medvedev et al.*, 2011a]. Overall, these results agree with the highly variable nature of GW fluctuations observed by MAVEN/NGIMS. However, in the majority of the calculated profiles, GWs happen to dissipate rapidly above $\sim$120 km: 75.7% of the harmonics demonstrate decreasing amplitudes, suggesting that the vast majority of the waves are being attenuated; only 5.7 % of waves show increasing amplitudes; and 18.6% of harmonics have already been completely dissipated below 120 km.

Further data-model comparison can be performed by analyzing the spatiotemporal variations of the modeled GW-induced density perturbations in the same manner as was done for the NGIMS/MAVEN observations shown in Figure 2. Local time, latitude, and altitude variations of ρ'/ρ_0 are presented in Figures 4a–c, respectively. In the calculations of the local time (panel a) and latitude (panel b) variations of the mean ρ'/ρ_0, altitude levels from 150–200 km are considered. It is seen that modeled values of ρ'/ρ_0 are generally smaller than those observed. GW-induced density perturbations peak at 6 LT, which partially agrees with MAVEN. The latitude distribution shows the general tendency of GWs to cause larger effects at higher latitudes.

There are several possible reasons for discrepancies between the simulated and observed density fluctuations. One is related to the uncertainties of GW sources in the lower atmosphere. Measurements of the GW field are difficult there due to its quasi-chaotic behavior and very small wave amplitudes. Even on Earth, the knowledge of GW sources is insufficient, and this is especially true for Mars. Second, wave propagation is strongly affected by the background wind. It was shown that the MCD fields, which are simply outputs from the general circulation model, are obviously inconsistent with the GW feedback on the mean flow [*Medvedev et al.*, 2011b], and that the winds in the upper mesosphere and thermosphere significantly alter when GW effects are included interactively in simulations [*Medvedev et al.*, 2011a, 2013]: they decrease, and even reverse, thus reducing the filtering and providing more favorable conditions for GW penetration to higher altitudes. Third, the profiles measured by NGIMS are the results of not only harmonics propagating from below and captured (to a certain degree) by the parameterization. GWs generated at higher altitudes and propagating significant horizontal distances are well known in the terrestrial thermosphere. Last but not least, the parameterization does not include fast infrasound waves, which, as has been shown in the works by *Walterscheid and Hickey* [2005] and *Walterscheid et al.* [2013], can effectively propagate to the upper thermosphere and attain significant amplitudes there. Despite these limitations, the presented calculations provide a valuable insight into the contribution to the detected variations of GWs of lower atmospheric origin.

6. Conclusions

For the first time, gravity wave-induced CO_2 density fluctuations in the Martian upper thermosphere (180–220 km) observed by the NGIMS instrument on board the NASA's MAVEN orbiter have been presented and discussed in the light of direct propagation and dissipation of harmonics of lower atmospheric origin. The main results and conclusions of this study are:

1. Evidence of wave-like perturbations is seen in the CO_2 number density observed by NGIMS during December 2014. The spatial scales of these perturbations, as measured along the MAVEN spacecraft trajectory, are consistent with the hypothesis that they are the manifestations of atmospheric gravity waves.

2. In the region studied here (180–220 km altitude, 60°–75° latitude and 2–10 hours local time), these waves have typical amplitudes of 20–30% relative to the background density.

3. An increase in the observed mean wave amplitude is seen with decreasing local time, which is similar to day-night variations observed by the ONMS mass spectrometer on Pioneer Venus. Some increase in the mean wave amplitude is seen as a function of latitude.

4. Numerical modeling with the extended gravity wave parameterization of *Yiğit et al.* [2008] using the Mars Climate Database fields for the MAVEN spatiotemporal conditions shows, in qualitative agreement with the observations, that GW propagation into the thermosphere is highly variable and that the instantaneous density fluctuations are $>$ 150% around 100 km and up to $50 - 100\%$ above 150 km.

Overall, the wave-like density perturbations have been observed at all altitudes up to 250 km. This is significantly higher than in previous observations of such waves on Mars, and even higher than in the theoretical estimates using the GW parameterization. More systematic measurements of density fluctuations in the thermosphere are required to constrain GW parameterizations and elucidate the physics and dynamical importance of these waves.

Acknowledgments. Modeling data supporting Figures 3 and 4 are available from EY (eyigit@gmu.edu). Mars Climate Database is available at http://www-mars.lmd.jussieu.fr/mars/access.html. This work was partially supported by NASA grant NNX13AO36G. The MAVEN project is supported by NASA through the Mars Exploration Program.

References

Bougher, S. W., J. M. Bell, J. R. Murphy, M. A. López-Valverde, and P. G. Withers (2006), Polar warming in the Mars thermosphere: Seasonal variations owing to changing insolation and dust distributions, *Geophys. Res. Lett.*, *33*, L02203, doi: 10.1029/2005GL024059.

Creasey, J. E., J. M. Forbes, and D. P. Hinson (2006a), Global and seasonal distribution of gravity wave activity in Mars' lower atmosphere derived from MGS radio occultation data, *Geophys. Res. Lett.*, *33*, L01803, doi:10.1029/2005GL024037.

Creasey, J. E., J. M. Forbes, and G. M. Keating (2006b), Density variability at scales typical of gravity waves observed in Mars' thermosphere by the MGS accelerometer,

Geophys. Res. Lett., *33*, L22814, doi:10.1029/2006GL027583.

Fritts, D. C., L. Wang, and R. H. Tolson (2006), Mean and gravity wave structures and variability in the Mars upper atmosphere inferred from Mars global surveyor and Mars odyssey aerobraking densities, *J. Geophys. Res.*, *111*, A12304, doi: 10.1029/2006JA011897.

Genio, A. D. D., G. Schubert, and J. M. Straus (1978), Gravity wave propagation in a diffusively separated atmosphere with height-dependent collision frequencies, *J. Geophys. Res.*, *84*, 4371–4378, doi:10.1029/JA084iA08p04371.

Kasprzak, W. T., A. E. Hedin, H. G. Mayr, and H. B. Niemann (1988), Wavelike perturbations observed in the neutral thermosphere of Venus, *J. Geophys. Res. Space Physics*, *93*(A10), 11,237–11,245, doi:10.1029/JA093iA10p11237.

Mahaffy, P., M. Benna, T. King, D. Harpold, R. Arvey, M. Barciniak, M. Bendt, D. Carrigan, T. Errigo, V. Holmes, C. Johnson, J. Kellogg, P. Kimvilakani, M. Lefavor, J. Hengemihle, F. Jaeger, E. Lyness, J. Maurer, A. Melak, F. Noreiga, M. Noriega, K. Patel, B. Prats, E. Raaen, F. Tan, E. Weidner, C. Gundersen, S. Battel, B. Block, K. Arnett, R. Miller, C. Cooper, C. Edmonson, and J. Nolan (2014), The neutral gas and ion mass spectrometer on the mars atmosphere and volatile evolution mission, *Space Sci. Rev.*, pp. 1–25, doi:10.1007/s11214-014-0091-1.

Medvedev, A. S., and E. Yiğit (2012), Thermal effects of internal gravity waves in the Martian upper atmosphere, *Geophys. Res. Lett.*, *39*, L05201, doi:10.1029/2012GL050852.

Medvedev, A. S., E. Yiğit, P. Hartogh, and E. Becker (2011a), Influence of gravity waves on the Martian atmosphere: General circulation modeling, *J. Geophys. Res.*, *116*, E10004,

doi:10.1029/2011JE003848.

Medvedev, A. S., E. Yiğit, and P. Hartogh (2011b), Estimates of gravity wave drag on Mars: indication of a possible lower thermosphere wind reversal, *Icarus*, *211*, 909–912, doi:10.1016/j.icarus.2010.10.013.

Medvedev, A. S., E. Yiğit, T. Kuroda, and P. Hartogh (2013), General circulation modeling of the martian upper atmosphere during global dust storms, *J. Geophys. Res. Planets*, *118*, 1–13, doi:10.1002/jgre.20163, 2013.

Medvedev, A. S., F. González-Galindo, E. Yiğit, A. G. Feofilov, F. Forget, and P. Hartogh (2015), Cooling of the martian thermosphere by CO_2 radiation and gravity waves: An intercomparison study with two general circulation models, *J. Geophys. Res. Planets*, *120*, doi:10.1002/2015JE004802.

Snowden, D., R. V. Yelle, J. Cui, J.-E. Wahlund, N. J. T. Edberg, and K. Ågren (2013), The thermal structure of Titan's upper atmosphere, I: Temperature profiles from Cassini INMS observations, *Icarus*, *226*, 552–582, doi:10.1016/j.icarus.2013.06.006.

Tolson, R., G. Keating, R. W. Zurek, S. W. Bougher, C. J. Justus, and D. C. Fritts (2007), Application of accelerometer data to atmospheric modeling during mars aerobraking operations, *J. Spacecraft Rockets*, *44*, 1172–1179.

Walterscheid, R. L., and M. P. Hickey (2005), Acoustic waves generated by gusty flow over hilly terrain, *J. Geophys. Res.*, *110*, A10307, doi:10.1029/2005JA011166.

Walterscheid, R. L., M. P. Hickey, and G. Schubert (2013), Wave heating and jeans escape in the martian upper atmosphere, *J. Geophys. Res. Planets*, *118*(2413–2422), 2169–9402, doi:10.1002/jgre.20164.

Yiğit, E. (2015), *Atmospheric and Space Sciences: Neutral Atmospheres*, SpringerBriefs in Earth Sciences, Springer, doi:10.1007/978-3-319-21581-5.

Yiğit, E., and A. S. Medvedev (2009), Heating and cooling of the thermosphere by internal gravity waves, *Geophys. Res. Lett.*, *36*, L14807, doi:10.1029/2009GL038507.

Yiğit, E., and A. S. Medvedev (2010), Internal gravity waves in the thermosphere during low and high solar activity: Simulation study., *J. Geophys. Res.*, *115*, A00G02, doi: 10.1029/2009JA015106.

Yiğit, E., and A. S. Medvedev (2015), Internal wave coupling processes in Earth's atmosphere, *Adv. Space Res.*, *55*, 983–1003, doi:10.1016/j.asr.2014.11.020.

Yiğit, E., A. D. Aylward, and A. S. Medvedev (2008), Parameterization of the effects of vertically propagating gravity waves for thermosphere general circulation models: Sensitivity study, *J. Geophys. Res.*, *113*, D19106, doi:10.1029/2008JD010135.

Yiğit, E., A. S. Medvedev, A. D. Aylward, P. Hartogh, and M. J. Harris (2009), Modeling the effects of gravity wave momentum deposition on the general circulation above the turbopause, *J. Geophys. Res.*, *114*, D07101, doi:10.1029/2008JD011132.

Yiğit, E., A. S. Medvedev, A. D. Aylward, A. J. Ridley, M. J. Harris, M. B. Moldwin, and P. Hartogh (2012), Dynamical effects of internal gravity waves in the equinoctial thermosphere, *J. Atmos. Sol.-Terr. Phys.*, *90–91*, 104–116, doi:10.1016/j.jastp.2011.11.014.

Yiğit, E., A. S. Medvedev, S. L. England, and T. J. Immel (2014), Simulated variability of the high-latitude thermosphere induced by small-scale gravity waves during a sudden stratospheric warming, *J. Geophys. Res. Space Physics*, *119*, doi: 10.1002/2013JA019283.

Yiğit, E., A. S. Medvedev, and P. Hartogh (2015), Gravity waves and high-altitude CO_2 ice cloud formation in the martian atmosphere, *Geophys. Res. Lett.*, *42*, doi: 10.1002/2015GL064275.

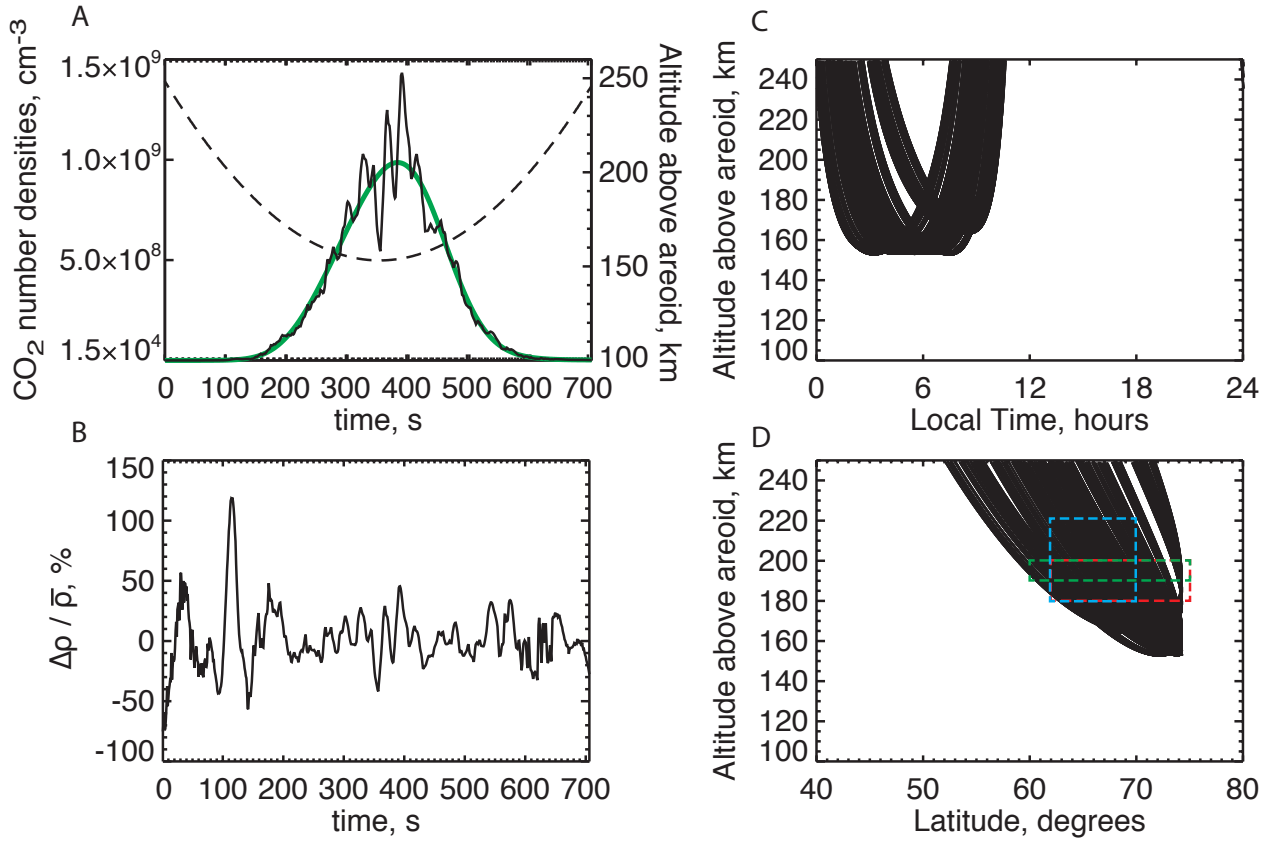

Figure 1. MAVEN orbital details: (a) The black dashed line shows the MAVEN spacecraft altitude as a function of time measured from the point at which the spacecraft passes 250 km altitude relative to the areoid on its inbound pass (18 December 2014, 18:41:04 UT). The solid black line shows the CO_2 number density measured by NGIMS during this periapsis pass. The solid green line shows the least-squares fit to the CO_2 number density described in the text; (b) shows the relative density perturbations during the same periapsis pass shown in panel (a); (c) and (d) show the sampling of the NGIMS data as functions of altitude, local time and latitude, for all the data from December 2014 that are used in this study, where each dot represents a single CO_2 density measurement. The red, blue, and green boxes are described in the text.

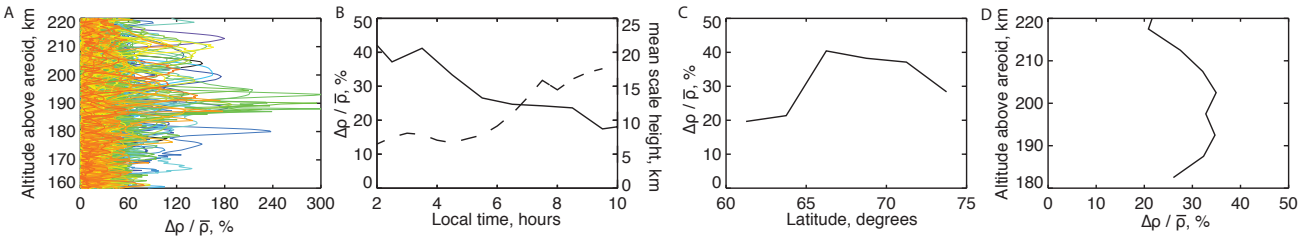

Figure 2. MAVEN observations of gravity wave-induced CO_2 density fluctuations in the upper thermosphere. (a) The relative density perturbations for all 78 profiles each displayed with different colors (both inbound & outbound); (b) the mean value of the absolute relative density perturbation (solid line) and the mean scale height (dashed line) as a function of local time, for within 180–200 km altitude above the areoid and $62° - 75°$N, from all periapsis passes during December 2014 described in the text. Values are shown in one-hour local time bins; (c) as (b), but as a function of latitude, for all data within 190–200 km altitude above the areoid and $60° - 75°$N. Values are shown in 2.5° latitude bins; (d) as (a), but as a function of altitude above the areoid, for all data within $62° - 70°$. Values are shown in 5 km altitude bins.

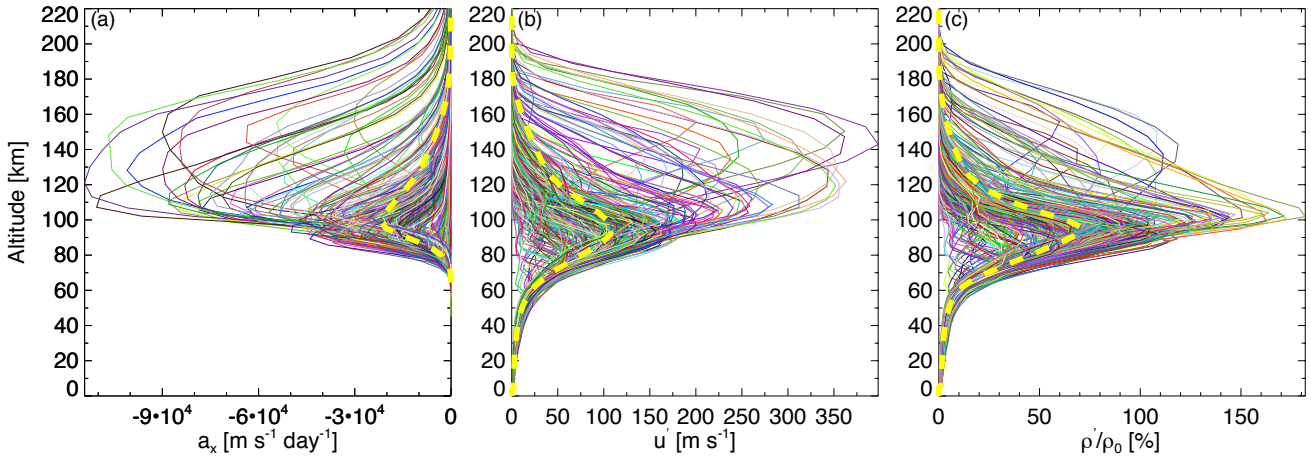

Figure 3. Altitude profiles of gravity wave effects calculated by the extended nonlinear gravity wave scheme of *Yiğit et al.* [2008] using the Mars Climate Database atmospheric fields as input for the observational conditions of MAVEN. Each profile is shown with a different color: (a) zonal GW drag a_x (m s^{-1} day^{-1}) with negative indicating westward drag; (b) rms wind fluctuations u' (m s^{-1}); (c) relative density perturbations ρ'/ρ_0 (%). The mean values of each parameter are shown with thick dashed yellow lines.

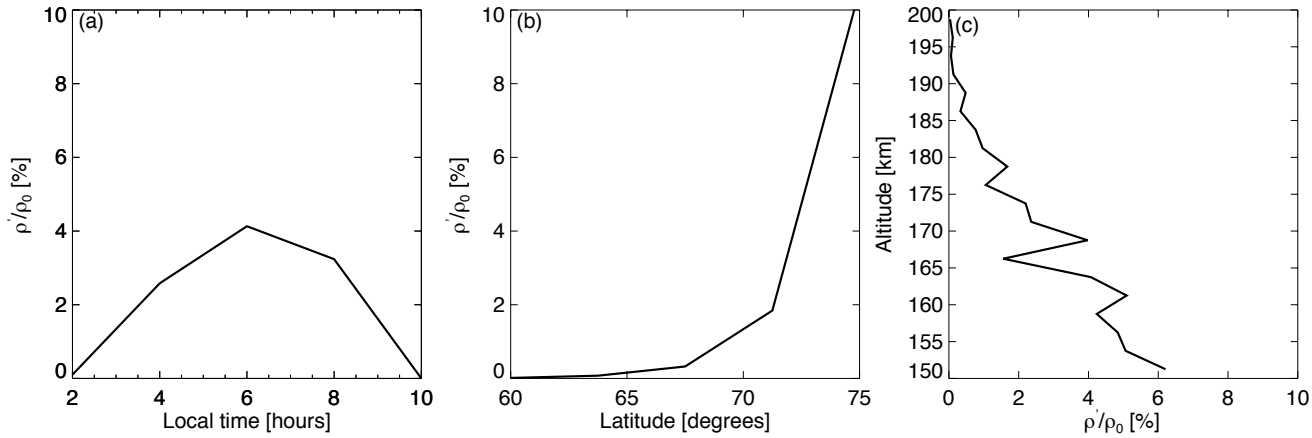

Figure 4. Modeled mean gravity wave-induced relative density perturbations ρ'/ρ_0 (%) that are presented in Figure 3 are binned for data between 150 and 200 km as a function of all (a) local times 2–10 hours; (b) latitudes 60°–75°. Altitude variation between 150–200 km for all local times and latitudes are shown in panel (c).